Optimum Conditions for Adsorptive Storage

Suresh K. Bhatia
Division of Chemical Engineering
The University of Queensland
Brisbane, QLD 4072, Australia

and

Alan L. Myers
Department of Chemical and Biochemical Engineering
University of Pennsylvania
Philadelphia, PA 19174-6393, U.S.A.

ABSTRACT

The storage of gases in porous adsorbents, such as activated carbon and carbon nanotubes, is examined here thermodynamically from a systems viewpoint, considering the entire adsorption–desorption cycle. The results provide concrete objective criteria to guide the search for the 'Holy Grail' adsorbent, for which the adsorptive delivery is maximized. It is shown that for ambient temperature storage of hydrogen and delivery between 30 bar and 1.5 bar pressure, for the optimum adsorbent the adsorption enthalpy change is 15.1 kJ/mole. For carbons, for which the average enthalpy change is typically 5.8 kJ/mole, an optimum operating temperature of about 115 K is predicted. For methane an optimum enthalpy change of 18.8 kJ/mole is found, with the optimum temperature for carbons being about 254 K. It is also demonstrated that for maximum delivery of the gas the optimum adsorbent must be homogeneous, and that introduction of heterogeneity, such as by ball milling, irradiation and other means, can only provide small increases in physisorption-related delivery for hydrogen. For methane heterogeneity is always detrimental, at any value of average adsorption enthalpy change. These results are confirmed with the help of experimental data from the literature, as well as extensive Monte Carlo simulations conducted here using slit pore models of activated carbons as well as atomistic models of carbon nanotubes. The simulations also demonstrate that carbon nanotubes offer little or no advantage over activated carbons in terms of enhanced delivery, when used as storage media for either hydrogen or methane.

Introduction

In recent years the increasing worldwide demand for energy has placed considerable strain on petroleum and other conventional sources such as coal. Combined with concerns about climate change arising from larger gas emissions associated with coal use, this has led to an acceleration of efforts to facilitate the development and utilization of technologies based on alternate sources such as natural gas and hydrogen. However, their application in the large mobile energy consumption sector, in conjunction with fuel cells or otherwise, has been impeded by the absence of safe and economical techniques for their on-board storage and this has been an area receiving much attention. Issues of safety and delivery pressure control preclude conventional ambient temperature storage as compressed gas, since pressures as high as 200-300 bar would be involved. Although the safety concern is mitigated by cryogenic storage or liquefaction (e.g. at 20 K for H_2), which involve substantially reduced pressures, this is not an economically viable option. Other options being considered are storage as chemisorbed hydrogen in hydrides [1], of both hydrogen and methane in clathrate hydrates [2] or as an adsorbed species within a suitable adsorbent [3-5]. For methane the DOE storage target is that of 150 v/v at 35 bar, which represents the volume of stored methane at standard conditions (298 K and 1 bar) per unit volume of vessel, though recently this has been revised to 180 v/v to achieve the same energy density as compressed natural gas. For hydrogen the target is set at 6.5% by weight of stored hydrogen and a volumetric density of 60 kg/m^3, to be achieved by 2010, with more ambitious targets of 9% by weight and volumetric density of 80 kg/m^3 set for 2015. While hydrides such as $NaAlH_4$, Li_3NH_4 and $LiBH_4$ are readily able to meet the 6.5 wt% DOE target for hydrogen, the high temperature needed for desorption, the stability of the hydrides, and high costs remain key impediments [3]. In the case of hydrates the targets have still not been achieved because of the prohibitively high pressures (in excess of 120

bar) needed for their formation [2]. Consequently, much effort has been devoted to investigating adsorptive storage as an alternative [5-15], whereby significantly higher storage densities comparable to that of the bulk fluid can be achieved at more moderate pressures.

Key to the success of adsorptive storage is the choice of suitable adsorbent and operating conditions. The early reports of over 60% by weight storage of hydrogen at ambient temperature and 112 bar pressure in carbon nanofibres [16], and of 14-20% in alkali doped carbon nanotubes at 1 bar pressure and temperatures from ambient to 673 K [7], have evoked much interest in carbons as the storage material. However, such extraordinary capacities have been criticized on fundamental grounds [17], and even questions of moisture contamination raised [18], with subsequent workers reporting much more modest storage of less than 5% by weight hydrogen even at cryogenic conditions of 77 K [3,6,12,19]. At the ambient temperature of 298 K and pressure of 30 bar the capacity is drastically less, in the range of 0.1-0.5 wt%. As a result a variety of inorganic materials have also been examined, such as zeolites and metal organic framework (MOF) materials or coordination polymers, in addition to other carbonaceous materials such as activated carbons and carbon nanotubes. Nevertheless, the DOE targets remain elusive despite the large amount of effort expended on adsorptive storage. For aluminosilicate zeolites H-Y and H-ZSM-5 hydrogen adsorption of less than 0.1% is reported at 300 K and 35 bar [19], while for sodalites maximum capacities of less than 4.8 wt% H_2 are predicted based on thermodynamic optimization [14], but even this is far from attainable at pressures below 30 bar. Similarly, aluminophosphates are shown to be unsuitable materials for methane storage [20]. MOF materials, now being more intensively studied [11,13,21-25], appear to show somewhat greater storage capacity, though they still fall short of DOE targets for H_2.

Among the family of isoreticular metal organic framework (IRMOF) materials IRMOF-8 appears the most promising adsorbent, with a reported capacity of 2 % by weight H_2 at 298 K and 10 bar pressure [11]. However, the subsequent results of Rowsell et al. [24], yielding a surface area of 1466 m^2/gm and hydrogen uptake of 0.75 wt% at 77 K and 1 bar for IRMOF-8, would suggest a significantly lower capacity. Indeed, based on the simulations of Garberoglio et al. [25] such materials are also well short of target, though at present there is some disagreement between simulation and experiment, and between data from different sources, with simulation generally predicting more modest capacities [25]. While this would suggest lack of reliable data with IRMOF's, the possibility of interaction potentials based on existing models being inaccurate cannot be discounted. For methane, IRMOF-6 [21] and specially designed but yet to be synthesized materials, IRMOF-992 and IRMOF-993, perform as well or better than carbon nanotubes, with storage capacities meeting the DOE target [13]. Thus, this family of materials does show potential, but is currently economically prohibitive. A further, though lesser, concern is the low density of these materials, which necessitates high container volumes.

While progress is being made, and capacities gradually improved, albeit still far from target in the case of hydrogen, the drive to meet DOE goals would appear to lack a well-defined objective. Thus, the necessary properties of the 'Holy Grail' adsorbent have not been objectively established. The general (mis)conception has been that an adsorbent with a sufficiently high specific volume and adsorption affinity is desirable, predicated on the assumption that this will increase storage capacity and therefore improve performance. However, too high an adsorption affinity will lead to large amount of residual adsorptive at the exhaustion pressure, and therefore to reduced delivery, while too low an affinity will also result in low delivery. Thus, an analysis of the entire adsorption-desorption cycle is

necessary in order to assess the utility of an adsorbent for on-board storage, rather than considering the storage capacity in isolation. Such an analysis has been suggested earlier by Matranga et al. [5], who determined the optimum value of the adsorption equilibrium constant necessary for maximizing delivery, based on the Langmuir isotherm. Since adsorption affinity, or the equilibrium constant, is related to the heat of adsorption one may surmise that it is this property that is important in the search for the right adsorbent. However, it should be noted that since the heat of adsorption generally varies with amount adsorbed, it is not the low coverage Henry's law value but the *average* heat over the coverage range of interest that is crucial. The average heat of adsorption of hydrogen on activated carbons is around 5.8 kJ/mole, which is close to the values reported by Bénard and Chahine [9] and to the average value for several polynuclear aromatic hydrocarbon molecules used as models of carbons [26]. Similar heats are observed in zeolites [27], but their pore volume is too small for practical application in storage. Little is known about the heat of adsorption of hydrogen in MOF structures, but the simulations of Sagara et al. [23] indicate a broad distribution of energies in the range 0-7 kJ/mole at room temperature for MOF-5 (also termed IRMOF-1), suggesting this to be a rather heterogeneous material. For the more promising IRMOF-8 the simulations of Garberoglio et al. [25] yield homogeneous behavior at 298 K, with a relatively constant isosteric heat of 4.39 kJ/mole, and heterogeneous behavior at 77 K, with the heat decreasing from 4.25 kJ/mole to about 3.5 kJ/mole as the pressure is increased to 90 bar. For single wall carbon nanotubes (SWNT's) of about 0.8 nm diameter the estimated average heat of adsorption of hydrogen, taken as that at 3% coverage, is about 8-9 kJ/mole [28], considering both endohedral and exohedral adsorption, but decreases to about 5.9 kJ/mole for 1.2 nm diameter tubes. The adsorption at ambient temperatures is expected to be almost entirely due to van der Waals interactions or physisorption [29], with chemisorption having prohibitively slow kinetics and requiring a

desorption temperature too high (>600 K) to make its exploitation practical. For methane in carbon nanotubes the low coverage heat is about 17-20 kJ/mole [13], and is somewhat higher than that for IRMOF's, where values in the region of 12-15.5 kJ/mole are reported for the most interesting structures [13]. Interestingly, silicalite has a high heat of adsorption for methane, of about 19.7 kJ/mole [13], attributable to its small pore size of about 0.6 nm, but its pore volume and surface area are too small for practical interest as a storage material.

From the above discussion it is evident that for hydrogen the heats of physisorption for the materials surveyed above are in the range of about 4-8 kJ/mole, while for methane the heats lie in the range of 12-19 kJ/mole, depending on adsorbent material. However, without an objective criterion in this regard it is not obvious whether these values are adequate or even promising.

Further, is a homogeneous or heterogeneous adsorbent more desirable? Attempts are being made at creating heterogeneities in various ways to enhance adsorption, particularly in carbons, but it is not established if this is an appropriate strategy. Among the various techniques alkali-metal doping of carbons and nanotubes [7] has been claimed to lead to 14-20 % by weight of hydrogen, but this has subsequently been suggested [18] as being due to moisture contamination. Defect creation in SWNT's and nanostructured graphites by mechanical means such as by ball-milling [30-34], as well as by ion irradiation [35], has also been attempted, but such defects have largely created chemisorptive trapping sites with desorption temperatures in the range of 600-950 K that are far too high to be of practical interest. Similar behavior has also been observed for nanocomposites obtained by the mechanical grinding of graphite with metals such as magnesium along with organic

additives [36]. Thus, the introduction of heterogeneities has not been successful, and it is not obvious if this is an appropriate or well-directed strategy. Indeed, no analysis of heterogeneity as a strategy for the storage-delivery cycle appears to have been made.

Based on the earlier discussion it is evident that carbons remain the most attractive candidates for physisorptive storage of both hydrogen and methane, considering their strong adsorption as well as low cost. Here we develop objective criteria for the desired heat of adsorption and level of heterogeneity for optimum performance of the storage delivery cycle. For a given adsorbent the optimum operating temperature of the cycle is also determined based on thermodynamic grounds, and application for the results to slit pore carbons as well SWNT's is discussed, with support from simulation.

Optimum Isosteric Heat and Temperature

As discussed above the current search for a suitable adsorbent for storage lacks a well defined objective in terms of the required strength of the adsorption interaction. To this end we consider a homogeneous adsorbent and the Langmuir isotherm

$$n = \frac{KPn_m}{1+KP} \tag{1}$$

where K is the equilibrium constant, n_m is the adsorption capacity and P is pressure. The Langmuir model is admittedly an approximation, but for a light gas such as hydrogen that is also weakly interacting, it provides sufficient accuracy over a wide range of pressures. Ideally, for maximizing delivery a cooperative isotherm, having a positive value of the second derivative $\left(\partial^2 n/\partial P^2\right)_T$ (Type III or Type V in the IUPAC classification [37]), is desirable. While such cooperative behavior may be observed for adsorption at subcritical conditions in mesopores and macropores, under supercritical conditions $\left(\partial^2 \mathrm{n}/\partial \mathrm{P}^2\right)_T$ is

always negative (Type 1 isotherm). Microporous materials such as zeolites and carbons always yield this behaviour, even under subcritical conditions. For storage applications involving hydrogen or methane, it is almost certainly the supercritical region that is of interest, and the Langmuir model provides the simplest yet sufficiently accurate isotherm for this region.

Upon equilibration at storage pressure P_1, the subsequent delivery at exhaustion pressure P_2 is given by

$$D(K, P_1, P_2) = \frac{KP_1 n_m}{1 + KP_1} - \frac{KP_2 n_m}{1 + KP_2} \tag{2}$$

It is readily determined that, at fixed P_1 and P_2, the delivery, D, is maximum for [5]

$$K = \frac{1}{\sqrt{P_1 P_2}} \tag{3}$$

Further, $K = e^{\Delta S^o / R} e^{-\Delta H^o / RT} / P_o$, where ΔH^o is the enthalpy change on adsorption, ΔS^o is the entropy change relative to the standard pressure P_o (1 bar), T is temperature and R is the ideal gas constant. It should be noted that in reality the differential enthalpy of adsorption will vary with coverage, or amount adsorbed, but for the Langmuir isotherm approximation in Eq. (1) the constant enthalpy change ΔH^o represents the average or integral heat of adsorption between P_1 and P_2, and its absolute value is equal to the isosteric heat. It then follows that for maximum delivery between P_1 and P_2 at given temperature T,

$$\Delta H^o{}_{opt} = T\Delta S^o + \frac{RT}{2} \ln\left(\frac{P_1 P_2}{P_o^2}\right) \tag{4}$$

As will be subsequently shown, for the adsorption of hydrogen, $\Delta S^o \cong -8R$ for a variety of adsorbents. For the delivery cycle reasonable values of adsorption and desorption pressures

may be taken as P_1 = 30 bar and P_2 = 1.5 bar respectively, which upon substitution in Eq.(4) yield $\Delta H^o_{opt} = -15.1$ kJ/mole at T = 298 K. Thus, for optimum delivery of hydrogen between pressures of 30 bar and 1.5 bar at 298 K, an adsorption enthalpy change of -15.1 kJ/mole is desired.

As indicated earlier, the isosteric heat of adsorption of hydrogen on carbons is typically about 5.8 kJ/mole, substantially less than the optimum value 15.1 kJ/mole required for maximum delivery at 298 K. However, if cryogenic conditions are acceptable then one may determine an optimum temperature of operation in the case of activated carbon, for which delivery is maximized, given the value of the isosteric heat of adsorption of 5.8 kJ/mole. Following Eq.(4), this temperature is obtained as

$$T_{opt} = \frac{\Delta H^o}{[\Delta S^o + (R/2)\ln(P_1 P_2 / P_o^2)]} \tag{5}$$

which provides T_{opt}=114.4 K, for P_1 = 30 bar, P_2 = 1.5 bar, $\Delta H^o = -5.8$ kJ/mole and $\Delta S^o = -8R$. Thus, for optimum performance of the delivery cycle using an activated carbon adsorbent an operating temperature of about 115 K is desirable. This is substantially lower than ambient temperature, and demonstrates the futility of current worldwide efforts at improving ambient temperature hydrogen storage capacity of carbons, and other materials with even lower isosteric heat. These conclusions will be further supported with simulations of the delivery in a subsequent section.

It may be noted here that values of the binding energy as high as 10 kJ/mole are predicted for interstitial hydrogen in C_{60} carbons [38], an extreme condition that nevertheless illustrates the maximum possible value of the heat for the most favorable sites in carbons.

This also shows that a value of the standard enthalpy change of the value of -15.1 kJ/mole is essentially unattainable in carbons.

The above concepts of optimum isosteric heat of adsorption and optimum temperature may also be applied to methane storage. In this case, as will be shown later, $\Delta S^o \cong -9.5R$ for a variety of adsorbents, and Eq. (4) yields $\Delta H^o = -18.82$ kJ/mole for a cycle operating between 30 bar and 1.5 bar at 298 K. This is consistent with the range of values found for methane in carbons, and close to that for some IRMOF's, as discussed earlier. Consequently, for methane efficient operation of the storage-delivery cycle should be feasible at near ambient temperatures. Indeed, for activated carbons a typical average value of the standard enthalpy change on adsorption is about 16 kJ/mole, based on which Eq. (5) provides an optimal temperature of 253.3 K. For IRMOF's where slightly lower values of the adsorption enthalpy change are encountered, the optimal temperature is expected to be lower. Given the low cost of activated carbon, there would appear to be little incentive for using IRMOF materials in this application.

Optimal Delivery from Carbons

For the optimal adsorbent, for which $K = 1/\sqrt{P_1 P_2}$, following Eq. (3), it is readily determined that the maximum delivery is 63.5% of the adsorption capacity, for P_1 = 30 bar, and P_2 = 1.5 bar. Considering activated carbon, to estimate the capacity we may assume that the carbon comprises of single graphene sheets, separated by slit micropores just wide enough to accommodate exactly two layers of the adsorptive (one layer near each wall), as depicted in Fig. 1. Such a carbon has a surface area of 2630 m^2/gm, which is the maximum possible value for ideal slit pore carbons [5,39]. Real carbons, of course, do have considerable short range disorder, and the slit-pore depicted in Figure 1 is therefore an

idealized case. The micropore size that can just accommodate two layers may be expected to have the maximum adsorptive packing density under supercritical conditions at which larger pores do not form multilayers. Even higher densities may be obtained at larger pore sizes, due to packing transitions [40,41] typical of Lennard-Jones (LJ) fluids, however very high pressures or low temperatures would be needed.

Studies with different adsorptives based on the LJ interaction model have shown that the pore size, measured center-to-center between carbon atoms in opposing planes, at which exactly two adsorptive layers can be accommodated is about $2.9\sigma_{fs}$ [40,41], where σ_{fs} is the value of the fluid-solid LJ interaction length scale parameter. For the case of hydrogen we use the value of 0.296 nm for the fluid-fluid parameter σ_{ff} [42], while for carbon we assume, following Steele [43], the solid-solid parameter value of σ_{ss} = 0.34 nm. Employing the Lorentz-Berthelot mixing rules we obtain the binary parameter, $\sigma_{fs,}$ which leads to a center-to-center pore width of 0.92 nm as the optimal value for hydrogen. Assuming 2-D hexagonal close packing of the LJ hydrogen, with spacing of $2^{1/6}\sigma_{ff,}$ the molecular area is estimated as 0.0956 nm^2. Given the area of 2630 m^2/gm, we now obtain the maximum hydrogen capacity of our idealized carbon as 9.2 wt%, which yields a maximum delivery of 5.8 wt % based on the maximum fractional delivery of 63.5%. Somewhat higher deliveries may be obtained for larger pore size carbons having larger pore volumes, at highly cryogenic conditions where multilayers can form, as will be subsequently shown. However, based on the present calculation it would appear that the DOE goals, considered as delivery rather than storage targets, cannot be met by physisorption in carbon, even under the most optimistic of conditions.

For the case of methane we may take σ_{ff} to be 0.381 nm, which yields an optimum pore width of 1.045 nm, and a molecular area of 0.158 nm^2, considering hexagonal close packing with spacing of $2^{1/6}\sigma_{ff}$.. Considering the surface area of 2630 m^2/gm, we obtain the maximum capacity as 44.24 wt%, and a maximum delivery of 28.1 wt%. To convert this into a volumetric capacity we first calculate the local microporosity, ε_μ, estimated as $(H\text{-}0.334)/H$, which represents the ratio of open pore width to center-to-center pore width, and obtain $\varepsilon_\mu = 0.680$. This local microporosity is that within regions having single layer graphene sheets separated by the micropores. Such microporous regions must be surrounded by larger macroporous regions that will serve to transport the adsorptive into the particle. Assuming a reasonable value of such macroporosity to be 26% of the particle volume (based on closed packing of spherical microporous domains), we obtain a particle density of 0.538 g/cm^3 considering the density of 2.27 g/cm^3 of graphite. This leads to a maximum delivery of 9.44×10^{-3} mol/cm^3. Assuming also the close packed porosity of 26% for the particle packing, and ideal gas conditions at 298 K, 1 bar pressure, we now obtain the maximum volumetric delivery as 173.1 v/v, which is only marginally lower than the most recent DOE target of 180 v/v. Thus, carbon would appear to be well suited for methane storage and delivery at near ambient temperature.

Effect of Heterogeneity

Considerable effort, outlined earlier, is being devoted to improving specific storage density in carbons, particularly in carbon nanotubes, by means of alkali metal doping, creating defects by ball milling or irradiation, and preparing composites, all of which may be viewed in the general context of introducing heterogeneities. To investigate whether this is an appropriate strategy we consider the Langmuir isotherm with a uniform distribution of ΔH^o, which leads to the Unilan model [44]

$$n = \frac{n_m}{2s} \ln\left[\frac{(1 + K_h e^{s} P)}{(1 + K_h e^{-s} P)}\right] \tag{6}$$

Here K_h is an equilibrium constant, determined at the mean value of ΔH^o, following

$$K_h = e^{\Delta S^o / R} e^{-\Delta \bar{H}^o / RT} / P_o \tag{7}$$

Further, the magnitude of the mean value of the enthalpy change is given by $(-\Delta \bar{H}^o) = (E_{\max} + E_{min})/2$, where E_{max} and E_{min} are the maximum and minimum values of --ΔH^o, which is uniformly distributed between these limits, and the parameter s represents a heterogeneity parameter given by $s = (E_{\max} - E_{\min})/2RT$. It is now possible to maximize the delivery between pressures P_1 and P_2, at fixed value of this heterogeneity parameter s, in a manner similar to that illustrated earlier for the Langmuir model. This leads to a result for K_h identical to Eq. (3), i.e. $K_h = 1/\sqrt{P_1 P_2}$. Similar to Eq. (4), we now obtain the optimum value of the mean standard enthalpy change as $\Delta \bar{H}^o_{opt} = T\Delta S^o + (RT/2)\ln(P_1 P_2 / P_o^2)$, which holds provided $-\Delta \bar{H}^o_{opt} / RT \geq s$, since E_{min} must be positive. When this inequality is not satisfied, i.e. $s > -[T\Delta S^o + (RT/2)\ln(P_1 P_2 / P_o^2)]$, the optimum value is given by the value of s. Thus, for a heterogeneous system following the Unilan model,

$$\Delta \bar{H}^o_{opt} = T\Delta S^o + \frac{RT}{2}\ln(P_1 P_2 / P_o^2), \text{ for } s \leq -\left[T\Delta S^o + \frac{RT}{2}\ln(P_1 P_2 / P_o^2)\right] \tag{8}$$

$$\Delta \bar{H}^o_{opt} = s, \text{ for } s > -\left[T\Delta S^o + \frac{RT}{2}\ln(P_1 P_2 / P_o^2)\right] \tag{9}$$

It is clear that the optimum value of the standard enthalpy change is the same as for a homogeneous system, suggesting that for the optimum adsorbent heterogeneity is detrimental for the storage delivery cycle. This is also intuitively obvious, because in a collection of independent adsorption sites, it is the optimal site that is most productive.

Thus, for maximum delivery every site must be independently optimal, i.e. the adsorbent must be homogeneous.

Figure 2 depicts the variation of delivery expressed as a fraction of the capacity, n_m, with heterogeneity parameter *s*, for various values of $-\Delta H^o/RT$, for both hydrogen and methane. For hydrogen, for which $\Delta S^o \cong -8R$, the value of $-\Delta H^o_{opt} / RT$ is 6.1 at 298 K, and Figure 2a shows that in this case any heterogeneity reduces delivery, supporting the above conclusion that the optimum adsorbent must be homogeneous. At this condition the delivery is about 63.5% of capacity. As will be subsequently shown, this corresponds to as much as 5-6 wt% delivery in the most optimistic case for carbon, attained at cryogenic conditions of about 100 K. However, for carbons, considering $-\Delta H^o$ to be 5.8 kJ/mole and $-\Delta H^o_{opt} / RT = 2.34$ at 298 K, there is some merit in heterogeneity (with *s* as large as 2.34) if *ambient* temperature operation is desired., although the maximum increase in delivery is not large, from about 9% to 14.2% of capacity. If the adsorption heat is increased to 9.91 kJ/mole (i.e. $-\Delta H^o_{opt} / RT = 4.0$ at 298 K) by creating heterogeneity through alkali metal doping or other methods, then a value of *s* as high as 2.5 is beneficial, as is evident from the curve for $-\Delta H^o_{opt} / RT = 4.0$ in Figure 2a, and increase in delivery to about 35% of capacity is possible. However, this delivery is still significantly smaller than that (63.5% of capacity) for the optimal condition, which is attained for the homogeneous adsorbent at 298 K having heat of adsorption of 15.1 kJ/mole, or the homogeneous carbon at 114 K having heat of adsorption of 5.8 kJ/mole. Even in this optimized scenario the maximum delivery is less than 6% by wt. hydrogen. Thus, it appears that efforts to introduce heterogeneity in carbons, by techniques such as ball milling or alkali metal doping are unlikely to result in

targets being achieved for hydrogen, though some incremental improvement in delivery is possible.

In the case of methane, for which $\Delta S^o \cong -9.5R$, the value of $-\Delta H^o_{opt} / RT$ is 7.6 at 298 K. Figure 2b depicts the variation in delivery with heterogeneity parameter, *s*, determined using the Unilan model, for various values of -$\Delta H^o/RT$. It is clear that heterogeneity is always detrimental in this case, and a homogeneous adsorbent is desired for any value of temperature or adsorption enthalpy change.

In summary, the objectives in the search for a suitable adsorbent are now fairly clear. In the case of hydrogen it is a *homogeneous* adsorbent operated at a temperature such that $-\Delta H^o_{opt} / RT = 6.1$. If the adsorbent is carbon, for which -ΔH^o ~ 5.8 kJ/mole, this yields an optimal temperature of about 115 K, while for ambient temperature operation an adsorbent for which the value of $\Delta H^o/RT$ is -15.1 kJ/mole is required. For methane, $-\Delta H^o_{opt} / RT = 7.6$, and if the adsorbent is carbon, in which case ΔH^o ~ 16 kJ/mole, the optimal temperature is about 254 K, while ambient temperature operation requires the value of $\Delta H^o/RT$ to be -18.8 kJ/mole. These results point to the difficulty of attaining DOE targets for hydrogen. However, it should be recognized that while the targets provide long-term goals for research outcomes in the area, their achievement is not the criterion determining commercial interest. Given an adsorbent material and the associated adsorption affinity, ultimately it is the economics that will decide its viability for use in on-board storage, even when DOE targets are not achieved. In what follows we analyze storage in activated carbons as well as carbon nanotubes, using grand canonical Monte

Carlo (GCMC) simulations to investigate the delivery and, in particular, to confirm the predictions of optimal temperature.

Simulation

GCMC simulation is a commonly used technique to study the properties of confined as well as bulk fluids, especially at supercritical conditions. The simulation is conducted in a constant volume system defined by a simulation box, in which the number of fluid particles, *N*, and configurational energy, *E*, are allowed to fluctuate at constant temperature and chemical potential. Random microstates are generated based on the well established Metropolis scheme [45], involving three types of moves, namely creation, deletion and displacement of fluid particles, with acceptance probabilities for the moves given by Adams algorithm [46]. Our simulations followed this commonly used procedure, with properties estimated by averaging over the microstates. Thus, the density of the system is defined by the mean number of particles per unit volume of the box. For the isosteric heat, we employ the widely used fluctuation formula [47]

$$q_{st} = k_B T - \frac{< NU > - < N >< U >}{< N^2 > - < N >< N >} \tag{10}$$

Where *N* and *U* are the number of particles and the total internal energy in any given configuration respectively, while $< \bullet >$ represents a configurational average. Further, since fugacity is the natural independent variable for GCMC, bulk fluid simulations were also performed to determine the corresponding bulk pressure. For this we used the virial expression

$$P = \frac{N k_B T}{V} + \frac{1}{3V} \left\langle \sum_{i<j} \mathbf{f}(\mathbf{r_{ij}}) \bullet \mathbf{r_{ij}} \right\rangle \tag{11}$$

where V is the volume of the simulation box and $\mathbf{f}(\mathbf{r_{ij}})$ is the force between two particles separated by the distance vector $\mathbf{r_{ij}}$. However, for hydrogen, for which quantum effects can be significant at low temperature the pressure was computed using a virial equation of state fitted to experimental PVT data.

Initially, simulations were performed for adsorption of hydrogen and methane in carbon slit pores, as well as for hydrogen in infinitely long cylindrical pores in amorphous silica, in order to determine the standard entropy change for hydrogen as well as methane adsorption. Subsequently, simulations were conducted to determine deliveries between 30 bar and 1.5 bar pressure for slit pore carbons, as well as carbon nanotubes, for various temperatures in the range of 77-298 K. In the case of cylindrical pores in silica the pore walls were considered infinitely thick and modeled as comprising 12 layers of close packed LJ sites. In all cases the LJ 12-6 potential is used to model the fluid-fluid as well as fluid solid interactions. The Lorentz-Berthelot (LB) mixing rules were used to estimate LJ parameters for the fluid-solid interaction. Table 1 lists the values of the LJ parameters used for the different components. The solid-solid parameters for silica are based on fit of argon isotherms at 87 K in MCM-41 [48], while for hydrogen we used the Buch [42] parameters. In all cases a cut-off distance of 1.5 nm was used in estimating potentials. The pore length was chosen sufficiently large so that the system had at least 200 fluid particles, and in each run a total of $8\text{x}10^6$ to $1.5\text{x}10^7$ configurations were sampled. Periodic boundary conditions were used in the axial direction in a cylindrical pore to simulate infinite length.

In the case of slit pores the Steele [43] 10-4 potential

$$\phi_{fs}(z,n) = 2\pi\rho_s\sigma_{fs}^2 \in_{fs} \left[\frac{2}{5}\left(\frac{\sigma_{fs}}{z}\right)^{10} - \left(\frac{\sigma_{fs}}{z}\right)^{4} \right] \tag{12}$$

was used to model the gas-solid interaction on a single plane, where z is the distance between an adsorbate molecule and the solid surface and ρ_s is the surface density of the carbon atoms on a graphene plane. The total potential in a pore of width H is now obtained by adding the contributions from each wall, based on Eq. (12), to obtain

$$\Phi_{fs}^{tot}(z) = \Phi_{fs}(z) + \Phi_{fs}(H - z) \tag{13}$$

Periodic boundary conditions in the x and y directions were used in modeling the interactions in slit pores. For graphite ρ_s has value 38.17 nm^{-2}, and $\in_{cc} / k$ has the value of 28 K [43], and these were assumed applicable to the LJ sites in activated carbon. Application to the interpretation of hydrogen adsorption data [9] on AX-21 activated carbon confirmed the applicability of these parameters for the gas-solid interaction.

Simulations of delivery were also conducted for the case of single walled carbon nanotubes, using an atomistic model of the tube with carbon atoms arranged on the surface of the tube in a hexagonal lattice. Tubes of four different diameters were considered, corresponding to chiral vectors (6,6), (9,6), (9,9) and (10,10), having diameters (measured between centers of carbon atoms) of 0.81 nm, 1.02 nm, 1.22 nm and 1.36 nm respectively. Of these only the (9,6) tube, whose framework is depicted in Figure 3a, is chiral. The nanotubes were organized on a square lattice, as depicted in Figure 3b, with spacing between tube surfaces of 0.9 nm. The simulations were conducted in a rectangular three dimensional unit cell, with periodic boundary conditions in all three directions.

Application to Experimental Data

While the C-C interaction parameters in Table 1 have been commonly employed for modeling the gas-solid interaction for methane on carbon, based on the LB mixing rules,

there appears little work on assessing their applicability for the case of hydrogen on carbon. To determine the parameters in this case we applied our GCMC simulations to the interpretation of the extensive data of Bénard and Chahine [9] for H_2 on AX-21 carbon at various temperatures (12 different temperatures) in the range of 77-298 K and pressures up to about 60 bar. In these simulations the aim was to determine the value of ε_{fs} for accurate matching of the gas-solid adsorption virial coefficient at the various temperatures. However, since the pore size distribution (PSD) is unknown, it was necessary to simultaneously also determine this distribution by jointly also fitting the whole isotherm at the various temperatures. To determine the virial coefficients we first fitted the Bénard and Chahine data by the virial isotherm [49]

$$\ln(P/n) = A + Bn + Cn^2 + ... \tag{14}$$

which provides the Henry law constant, K_H as exp(-A). The gas-solid virial coefficient B_{fs} is theoretically defined as [43]

$$B_{fs} = \int e^{-\phi_{fs}(\mathbf{r})/k_B T} d\mathbf{r} \tag{15}$$

where the integration is performed over the volume of the adsorbent. In terms of the Henry Law coefficient this is also given as

$$B_{fs} = K_H RT = e^{-A} RT \tag{16}$$

so that the experimental value of B_{fs} is readily determined from the fitted value of A. Application of Eq. (14) to the Bénard and Chahine data yielded excellent fit with an average error of 2.5%, while utilizing only the first two terms of the expansion. This is indicative of the relatively weak nature of the H_2-H_2 interaction, compared to the C-H_2 interaction. In this fit the isotherm was corrected for excess, as is appropriate to experimental data, using the pore volume as an additional fitting parameter.

The determination of the theoretical value of B_{fs} by means of Eq. (15) requires some assumption about the structure of the carbon. We considered the structure as comprising of pores having sizes H_1 = 0.755 nm, H_2 = 1.08 nm, H_3 = 1.44 nm and H_4 = 1.76 nm, based on recent observations [50] that peak micropore sizes are nearly the same for most carbons, and have these values. Since AX-21 is a super-high surface area carbon, with an area close [9] to the slit pore based maximum possible value of 2630 m^2/g, we consider its structure as comprised of single sheet walls, so that

$$\int_0^\infty \frac{2}{H} f(H) dH = 2630 \text{ m}^2 / g \tag{17}$$

where $f(H)$ is the PSD. With the integrals discretized at the above four sizes, Eqs. (15) and (17) yield

$$B_{fs} = \sum_{i=1}^{4} \frac{v_i}{H_i} \int_0^{H_i} e^{-\phi_{fs}(z)/k_B T} dz \tag{18}$$

$$\sum_{i=1}^{4} \frac{v_i}{H_i} = 1.315 \tag{19}$$

Where v_i is the specific pore volume (cm^3/g) at pore width H_i (nm). Here both v_i and H_i correspond to the space between centers of carbon atoms in the opposing single sheet walls of the slit pore. The specific open pore volume at any pore size, V_{pi} (cm^3/g), is given as

$$V_{p,i} = v_i \frac{(H_i - 0.334)}{H_i} \tag{20}$$

Combining Eqs. (19) and (20), the total specific open pore volume, V_p (cm^3/g), is obtained as

$$V_p = \sum_{i=1}^{4} v_i - 0.4392 \tag{21}$$

Theoretical values of B_{fs} and the GCMC generated isotherms were simultaneously fitted to their experimental counterparts using nonlinear regression with ε_{fs}/k_B, v_1, v_2 and v_3 as fitting parameters, and v_4 determined from Eq. (19). In actual implementation the fitting was performed for v_1, v_2 and v_3 at various values of ε_{fs}/k_B, and the value of ε_{fs}/k_B for minimum fitting error was subsequently determined. The error, E, of the fit error is defined using a combination of isotherm, excess delivery and virial coefficient points:

$$E = \sum_{i=1}^{12}\sum_{j=1}^{4}(n_{ij}^{\exp} - n_{ij}^{sim})^2/(n_{ij}^{\exp})^2 + \sum_{i=1}^{11}(B_{fs,i}^{\exp} - B_{fs,i}^{th})^2/(B_{fs,i}^{\exp})^2 + \sum_{i=1}^{12}(D_i^{\exp} - D_i^{sim})^2/(D_i^{\exp})^2 \quad (22)$$

in which the dummy variable i corresponds to temperature points and j to pressure points. For the virial coefficient the data at the lowest temperature of 77 K was not utilized because of greater uncertainty at this point. To reduce the computational load, the isotherm was fitted at only four points at each temperature, utilizing also an additional point for the delivery (between 30 bar and 1.5 bar) at each temperature. The latter was obtained from the virial fit of excess isotherms, which is accurate to within 2.5% and can essentially be considered experimental data.

Figure 4 depicts the fitting results for the gas-solid virial coefficients (Fig. 4a) and the excess isotherms (Fig. 4b) at various temperatures, showing good agreement in both cases. The value of the mean internal energy change ΔU (relative to an isolated H_2 molecule *in vacuo*), estimated from the slope of the linear correlation of the dashed line in Figure 4a is obtained as -4.52 kJ/mole, leading to an isosteric heat ($-\Delta U + RT$) of 6.08 kJ/mole at the mean temperature of 187.5 K (mid-point over the 77-298 K range), close to the typical value of 5.8 kJ/mole discussed earlier. For the fits excess isotherms from experiment were corrected to absolute isotherms using the calculated pore volume based on Eq. (20). The

fitting results for the center-to-center and the corresponding open pore volumes at the different pore sizes are given in Table 2, and yield a total open pore volume of 1.01 cm^3/gm, based on the hydrogen adsorption isotherms. The fitted value of ε_{fs}/k_B was 30.87 K. This is very close to the value of 30.95 K, expected based on the LB mixing rules and the value of ε_{cc}/k_B given in Table 1. Accordingly, the value of ε_{cc}/k_B in Table 1 was adopted for this study.

It may be noted that in the calculations reported above the quantum effect has not been considered for hydrogen. While such an effect is expected at low temperatures [51], at the lowest temperature of 77 K used by Bénard and Chahine this is not likely to be large. Nevertheless, since we have fitted experimental data, this effect is implicitly imbedded in the value of the gas-solid interaction parameter obtained. Indeed the good prediction of the data at 77 K in Figure 4b supports the approach. As an alternative we also performed fitting of the data using the Feynman-Hibbs [52] variational formulation of the effective quantum potential, for the gas-solid interaction. This yielded essentially the same fitting error with very similar results, but with ε_{fs}/k_B = 31.73 K. The slightly higher value is anticipated in view of the fact that quantum uncertainty leads to an effective swelling of the hydrogen, and reduces the effective magnitude of the potential energy. For our purposes, therefore, the effective classical potential imbedding the quantum effect suffices.

Figure 5 depicts the comparison of variation of experimental and calculated delivery with temperature, showing excellent agreement. In both cases the optimum temperature is about 100 K, slightly lower than the theoretical value of 115 K for carbon discussed above. Such reduction in optimum temperature is, however, to be anticipated in view of the effect of heterogeneity, as a result of which large pores reduce the heat of adsorption. Thus, based

on the internal energy change of -4.52 kJ/mole, at 100 K the heat of adsorption is estimated to be 5.35 kJ/mole, which leads to an optimum temperature of about 106 K. Further, at the optimum temperature of about 100 K the maximum delivery is only about 3.4 wt%, significantly less than the maximum delivery of about 5.8 wt% estimated above, despite the isosteric heat of 6.08 kJ/mole. This is due to the effect of heterogeneity, evident in the fitted pore size distribution given in Table 2.

Entropy Change on Adsorption

Our determination of the optimal value of $-\Delta H^o/RT$ has been based on the assumption that $\Delta S^o \cong -8R$ for the adsorption of hydrogen, and $\Delta S^o \cong -9.5R$ for the adsorption of methane. These values have been estimated based on Langmuirian analysis of simulation based adsorption isotherms on slit pores in carbon as well as cylindrical pores in silica, together with the thermodynamic formula $K = e^{\Delta S^o/R} e^{-\Delta H^o/RT} / P_o$. Figures 6 (a) and (b) depict the isotherms of hydrogen in carbon slit pores of different sizes at 100 K and 298 K respectively, plotted on Langmuirian coordinates, while Figure 6 (c) gives the isotherms in cylindrical silica pores at 298 K. These isotherms show excellent linearity, providing strong evidence for the relative weakness of the H_2-H_2 interaction and validity of the Langmuir model, thereby justifying our analysis of optimal delivery. At 100 K, some deviation from linearity occurs above about 35 bar pressure, attributed to increasing importance of fluid-fluid interactions. Table 3 provides the values of equilibrium constants obtained from the Langmuir plots in Figure 6, as well as the isosteric heats obtained from simulation and the corresponding values of $-\Delta S^o/R$. These results support the value of $\Delta S^o \cong -8R$ as a reasonable value for hydrogen adsorption, except at very small pore size. Thus, in silica, at the pore diameter of 0.65 nm the value of $-\Delta S^o / R$ increases to 8.95. This is attributed to the strong confinement at this pore size, with the hydrogen being

essentially a one dimension fluid. The relatively weak variation of $-\Delta S^o / R$ and its slightly smaller value at the other pore sizes in Table 3 may be interpreted as being due to similar degree of confinement. In support, it may be noted that even larger values of -$\Delta S^o/R$, approaching the bulk value of -10.5 associated with Trouton's rule [53], have been reported for the highly confined spaces of zeolites [27,54] and for surfaces of metals where strong adsorption occurs [55]. Nevertheless, for most carbons, where pore sizes are typically larger than those of zeolites, the approximation $\Delta S^o \cong -8R$ would appear reasonable. As will be subsequently demonstrated this value of ΔS^o is also appropriate for endohedral (internal) adsorption in carbon nanotubes.

Figure 6 (d) depicts Langmuirian plots for methane in carbon pores of various sizes at 298 K. In this case due to the significantly higher equilibrium constants, and appearance of nonlinearity at lower pressures, it was found more appropriate to plot the isotherms in the alternate coordinates used. From the results given in Table 3 it is evident that a value of $\Delta S^o \cong -9.5R$ is a reasonable approximation for methane at ambient temperature, which has been shown to be near the optimal value for methane storage on carbon.

Hydrogen Delivery from Slit Pore Carbons

Simulations were next conducted for the temperature variation of delivery between 30 bar and 1.5 bar pressure for hydrogen from homogeneous activated carbons having various pore widths. For the calculation, pore densities from simulation which are based on center-to-center pore volume, were converted to specific amounts (per unit mass of carbon) using the specific center-to-center pore volume (in cm^3/g)

$$v = 1.315H \tag{23}$$

which follows from eq. (19). Figure 7 (a) depicts the results for the absolute delivery from the micropores as a function of temperature for several slit widths. Clear evidence of an optimum temperature for maximum delivery at any slit width is seen, supporting the earlier analysis, with the optimum temperature decreasing with increase in slit width. This is to be expected, because of the decrease in isosteric heat with slit width. Further, at pore widths of 0.9 nm or 1.08 nm, that are typical for activated carbons, the optimal temperature is about 100 K, which is consistent with our earlier observation of 115 K as being optimal for carbons. Figure 7 (b) depicts the variation of isosteric heat with temperature for the different slit widths, and the locus of the optimum, following Eq. (4). Based on our analysis, the intersection of the latter with the isosteric heat curve at any size provides the optimal temperature at that size. This is readily confirmed for the three smaller sizes, by comparison with the temperatures of maximum delivery in Figure 7 9 (a). At the two highest sizes of 1.44 nm and 1.76 nm the optima occur near 77 K, which is the lowest temperature examined, and are therefore not evident in Figure 7 (a).

It has earlier been shown that the maximum hydrogen delivery from carbons is about 5.8 % by weight (i.e. 28.8 mol/kg), and this is borne out by Figure 7 (a), where maximum values of about this magnitude are seen near the optimal temperature of about 100 K. Slightly higher values can be observed for the two larger pore size carbons, but at very low temperatures of 77 K. From an excess delivery point of view, the maximum values are even lower, as seen in Figure 7 (c), further confirming the difficulty in meeting DOE targets of over 6.5 % by weight delivery of hydrogen with this material.

An interesting measure of the effectiveness of the storage delivery cycle is the enhancement factor, defined as the ratio of delivery from an adsorbent-packed container to that from an

identical one filled with bulk gas, operating between 30 and 1.5 bar. To determine this factor we consider a container packed with activated carbon with a bed voidage of ε_b, and assume the carbon to comprise of macroporosity ε_m, in which the fluid phase density is that of the bulk fluid. The volume of the micropore phase per unit volume of bed is then $(1-\varepsilon_m)(1-\varepsilon_b)$. Considering uniform micropore width of H (nm), we now obtain the total delivery per unit volume of container as

$$D_{tot} = [\varepsilon_b + \varepsilon_m(1-\varepsilon_b)]D_{bv} + \frac{(1-\varepsilon_m)(1-\varepsilon_b)D}{1.315H} \tag{24}$$

leading to the enhancement factor

$$E = [\varepsilon_b + \varepsilon_m(1-\varepsilon_b)] + \frac{(1-\varepsilon_m)(1-\varepsilon_b)D}{1.315HD_{bv}} \tag{25}$$

where D_{bv} is the delivery per unit volume from the bulk gas, and D is the delivery per unit mass of carbon from the micropore adsorbate. Here we have used Eqs. (23) for the specific micropore volume (center-to-center volume between carbon planes), and taken $\varepsilon_b = \varepsilon_m = 0.26$ (the close packed value). Figure 7 (d) depicts the variation of enhancement factor with temperature, for the homogeneous carbons of various pore sizes. It is evident that the maximum enhancement factor possible is about 3.1, attained for the 0.9 nm pore width carbon at about 110 K. A slightly lower result is obtained for the 1.08 nm and 0.755 nm carbons, while the larger pore widths of 1.44 nm and 1.76 nm, as well as the smaller pore width of 0.755 nm, yield significantly lower enhancement factors. Thus, the 0.9 nm pore width carbon utilizes the container volume most effectively, though the higher optimal temperature of about 150 K for the 0.755 nm carbon may possibly make this a more attractive option. Nevertheless, it should be noted that the enhancement factors determined here are based on the densest possible packing of spheres, with a void fraction of 26%. In practice the particles will not be spherical but irregular, and lower packing efficiencies will

be attained, typically with 30-35% porosity,, which will reduce enhancement factors slightly.

Hydrogen Delivery from Single-Walled Carbon Nanotubes

In the case of carbon nanotubes, initially simulations were conducted to determine the endohedral or internal adsorption of hydrogen in the tubes. For this a one-dimensional gas-solid potential energy profile was used, obtained by angular and lengthwise averaging of the three dimensional potential energy profile at any radial position. In the calculations we assumed ε_{fs}/k_B = 30.95, as was found appropriate for the AX-21 data of Bénard and Chahine [9]. Such a one dimensional profile is justified on the grounds that nanotubes have a rather smooth potential energy landscape, arising from the very small spacing (0.142 nm) between the centers of the covalently bonded carbon atoms, compared to their van der Waals .diameter (0.34 nm). Figure 8 (a) depicts the temperature variation of the delivery obtained based only on the endohedral adsorption in nanotubes of various diameters. As in the case of slit pore carbons, clear evidence of optimal temperature is seen, with the optimal value increasing from 113 K for the (10,10) nanotube of 1.36 nm diameter to about 213 K for the (6,6) tube having 0.81 nm diameter, as the tube size decreases. These temperatures are somewhat higher than those observed earlier for slit pores, which is attributable to the larger enthalpy changes for the endohedral adsorption in nanotubes. Figure 8 (b) depicts the variation of isosteric heat of adsorption with temperature for the different nanotubes, confirming the larger enthalpy change. Also shown in the figure is the locus of optimum delivery, based on Eq. (4) and $\Delta S^o \cong -8R$, whose intersections with the heat curves determine the optimal temperatures. The optimal temperatures thereby determined are completely consistent with the maxima in Figure 8 (a), indicating that the approximation $\Delta S^o \cong -8R$ is suitable also for this case.

The magnitudes of the deliveries based on endohedral adsorption alone, seen in Figure 8 (a) are significantly less than those from single sheet slit pore carbons, shown in Figure 7 (a). This is due to the fact that in the latter case adsorption occurs on both sides of the graphene sheet, while endohedral adsorption in nanoutubes occurs on one side of the wall only. Accordingly, one expects that simultaneous exohedral (external) as well as endohedral adsorption in nanotubes, as is expected in real systems, will significantly enhance the delivery. Figure 9 (a) depicts the results of such simulations, described earlier, for nanotubes packed in a square array, and spaced 0.9 nm apart, In all the nanotubes the of different sizes examined it is seen that the optimal temperature is significantly reduced, and less than 77 K. This is due to the highly inhomogeneous nature of the interstitial pore space in the nanotube array, depicted in Figure 3 (b), which is increasingly filled at the low temperatures. As a result the average isosteric heats between the filling and exhaustion pressures decrease strongly with decrease in temperature. This decrease is largely due to the higher loading at lower temperatures, and only partly due to the effect of temperature reduction. In the case of the smallest diameter tube (0.81 nm diameter), for example, the average isosteric heat between these pressures (*not* at constant loading) obtained from simulation using Eq. (10) decreases from about 6.4 kJ/mole at 298 K to about 3.65 kJ/mole at 77 K. In the latter case the optimal temperature would be obtained as 72 K for a homogeneous adsorbent, but is somewhat lower in the present case because of the heterogeneity of the interstitial space. For the larger tubes the optimal temperature would be expected to be even lower. In comparison to slit pore activated carbons, where higher optimal temperatures have been found, it would appear that carbon nanotubes are less attractive. Indeed, even the absolute deliveries of about 23 mole/kg or 4.6 wt.% at 100 K are lower than the amounts of about 28 mole/kg, or 5.7 wt % obtained for activated carbons

at this temperature. Nevertheless, it would appear that the nanotubes in the square array chosen here can make more efficient use of the space, as is evident from their slightly higher enhancement factors, depicted in Figure 9 (b). Here the enhancement factor is calculated as the ratio of delivery from the simulation box packed with nanotubes, to the delivery from the empty box filled with bulk gas. In this case an optimal temperature near 100 K is evident for the two largest diameter tubes, with enhancement factors of about 4. However, some reduction in enhancement is likely in comparison to the results in Figure 9 (b) in view of dead spaces created in supporting nanotube bundles in a container, as transport in a fully packed container would be a serious bottleneck for delivery.

Methane Delivery from Slit Pore Carbons

For the case of methane in slit pore carbons, we have shown that the optimum temperature is about 254 K, given the typical standard enthalpy change of about -16 kJ/mole. Our simulations for methane delivery, depicted in Figure 10, confirmed this result. While the optimal temperature decreases with increase in pore width, as seen in Figure 10 (a), for the pore width of 1.08 nm, which is representative of the modal pore width in most activated carbons, the optimal temperature is about 253 K. At this pore width the maximum absolute delivery of 15.2 mole/kg, or 24.3 wt%, is consistent with our estimate of 28.1 wt% maximum delivery at the optimal condition. At larger pore widths the maximum delivery does increase, but at the cost of lower optimal temperature. Figure 10 (b) depicts the variation of isosteric heat, or magnitude of standard enthalpy change when interpreted in terms of the Langmuir isotherm, with temperature at the different pore widths. The optimal temperature at any pore size, obtained from the intersection of the heat curve with the locus of the optimum, is seen to be consistent with that in Figure 10 (a), again confirming the

applicability of our Langmuir isotherm-based analysis with the approximation of $\Delta S^o \cong -9.5R$ for methane adsorption.

Figure 10 (c) depicts the excess deliveries as a function of temperature, for the different pore sizes. In this case, at the pore width of 1.08 nm, the excess delivery is reduced to about 22.1 wt %, which corresponds to a volumetric delivery of about 136 v/v. If the targets are interpreted on an excess delivery basis, then the value of 136 v/v is significantly less than desired (180 v/v), and a larger pore width is advantageous, though requiring lower temperature, as is evident in Figure 10 (a) or 10 (c). Nevertheless, maximum volumetric efficiency is obtained for the pore width of about 1.08 nm, as is evident from the enhancement factors depicted in Figure 10 (d). These values are somewhat larger than those for hydrogen delivery from slit pore carbons, depicted in Figure 7 (d), predominantly due to the stronger interaction of methane with carbon. Indeed, maximum enhancement is obtained at about 273 K at the pore width of 1.08 nm, and from an economic viewpoint this may well be the most appropriate condition for methane storage and delivery from activated carbon. However, as indicated earlier for the case of hydrogen, actual enhancement factors will be slightly lower because of particle shape irregularities and lower packing efficiencies.

Methane Delivery from Single Walled Carbon Nanotubes

Figure 11 (a) depicts the absolute methane delivery as a function of temperature, for carbon nanotubes of different sizes, obtained from our atomistic simulations considering both endohedral and exohedral adsorption for tubes placed in a square array and spaced 0.9 nm apart. The optimum temperature is about 233 K for the largest nanotube examined, having 1.36 nm diameter, and decreases to about 213 K for the three other smaller sizes. These

temperatures are lower than the value of 254 K established here for a typical activated carbon, and attained for a homogeneous carbon having 1 nm pores, predominantly due to the heterogeneity of the interstitial space in which the exohedral adsorption occurs. Further, the maximum deliveries range between 14 and 15 mole/kg, which while comparable to the activated carbon of 1. nm, are lower than the maximum deliveries for larger pore width carbons, as seen in Figure 10 (a). These results would suggest that , as in the case of hydrogen, carbon nanotubes have no advantages over activated carbon from the viewpoint of methane delivery. Nevertheless, as for hydrogen they appear more efficient in terms of utilization of the container volume, as is evident from the slightly higher enhancement factors depicted in Figure 11 (b). In practice however the enhancement factor will be significantly lower because of dead spaces in the container, which will be necessary to allow access to the nanotubes in order to mitigate transport resistances that would arise in very large bundles.

Conclusions

The thermodynamic requirement for an adsorbent capable of storing hydrogen at ambient temperature is a heat of adsorption of hydrogen equal to 15.1 kJ/mol. This value for the heat of adsorption is optimal with respect to the affinity of hydrogen: strong enough to store a large amount of hydrogen gas at the charging pressure (about 30 bar) but weak enough to release most of that hydrogen at the discharge pressure (about 1.5 bar).

Current research targets of adsorption of 6.5% by weight of hydrogen at high pressure fail to consider the complete adsorption cycle of charging and discharging. Achievement of the target will be meaningless unless most of the gas is released reversibly at the discharge

pressure. It is shown that the maximum *delivered* gas is about 63.5% of the total capacity of the adsorbent at high pressure, even for an optimal cycle.

For carbons, the heat of adsorption of hydrogen is only about 6 kJ/mol, so adsorption of hydrogen on carbon in any form (active carbon or carbon nanotubes) is too weak for storing hydrogen at ambient temperature. The optimal temperature for maximizing the delivery of hydrogen adsorbed on carbon is 115 K, which is far below the desired ambient temperature of 300 K.

The ideal adsorbent is energetically homogeneous, that is, the isothermal heat of adsorption should be constant with loading for optimal delivery. Energetic heterogeneity in any form is detrimental to adsorptive storage of gas.

The above conclusions are strongly supported by extensive experimental data and simulations.

Acknowledgement

The authors are grateful to Dr. P. Bénard, Université du Québec à Trois-Rivieres, for providing their extensive data on the adsorption of hydrogen on AX-21. We are also grateful to Dr. Anilkumar, The University of Queensland, for useful discussions and help with simulation code development. Support of the research at the University of Queensland by a grant from the Australian Research Council is also acknowledged.

References

1. Hu, Y.H.; Yu, N.Y.; Ruckenstein, E. *Ind. Eng. Chem. Res.* **2004**, *43*, 4174.

2. Lee, H. ; et al. *Nature* **2005**, *434*, 743.

3. Schlapbach, L.; Züttel, A. *Nature* **2005**, *414*, 353.

4. Orimo, S.; et al. *J. Alloys Comp.* **2003**, *356-357*, 716.

5. Matranga, K.R.; Myers, A.L.; Glandt, E.D. *Chem. Eng. Sci.***1992**, *47*, 1569.

6. Chahine, R.; Bose, T.K. *Int. J. Hydrogen Energy* **1994**, *19*, 161.

7. Chen, P.; Wu, X.; Lin, J.; Tan, K.L. *Science* **1999**, *285*, 91.

8. Nijkamp, M. G.; et al. *Appl. Phys. A.* **2001**, *72*, 619.

9. Bénard, P.; Chahine, R. *Langmuir* **2002**, *17*, 1950.

10. de la Casa-Lillo, M. A.; et al. *J. Phys. Chem. B.* **2002**, *106*, 10930.

11. Rosi, N.L.; et al. *Science* **2003**, *300*, 1127.

12. Nechaev, Y. S.; Alekseeva, O.K. *Russ. Chem. Rev.* **2004**, *73*, 1211.

13. Düren, T.; Sarkisov. L.; Yaghi, O.; Snurr, R. *AIChE J.* **2004**, *20*, 2683.

14. van den Berg, A. W. C.; et. al. *Microporous and Mesoporous Materials* **2005**, *78*, 63.

15. Lazano-Castello, D.; et al. *Fuel* **2002**, *81*, 1777.

16.Chambers, A.; Park, C.; Baker, R.T.K.; Rodriguez, N. M. *J. Phys. Chem. B.* **1998**, *102*, 4253.

17. Cracknell, R. F. *Phys. Chem. Chem. Phys.* **2001**, *3*, 2091.

18. Yang, R.T. *Carbon* **2000**, *38*, 623.

19. Takagi, H.; et al. *Mat. Sci. Eng.* **2004**, *B108*, 143.

20. Cracknell, R. F.; Gubbins, K.E. *J. Mol. Liq.* **1992**, *54*, 261.

21. Eddaoudi, M.; et al. *Science* **2002**, *295*, 469.

22. Pan, L.; et al. *J. Am. Chem. Soc.* **2004**, *126*, 1308.

23. Sagara, T.; Klassen, J.; Ganz, E. *J. Chem. Phys.* **2004**, *121*, 12543.

24. Rowsell et al., J. L. C; et al. *J. Am. Chem. Soc.* **2004**, *126*, 5666.

25. Garberoglio, G.; Skoulidas, A.I.; Johnson, J.K. *J. Phys. Chem. B.* **2005**, *109*, 13094.

26. Heine, T.; Zhechkov, L.; Seifert, G. *Phys. Chem. Chem. Phys.* **2004**, *6*, 980.

27. Areán, C. O.; et al. *Chem. Phys. Lett.* **2003**, *370*, 631.

28. Cheng, H.; et al. *J. Phys. Chem. B.* **2005,** *109*, 3780.

29. Li, J.; et al. *J. Chem. Phys.* **2003**, *119*, 2376.

30. Orimo, S.; et al. *Appl. Phys. Lett.* **1999**, *75*, 3093.

31. Orimo, S.; et al. *Metals Mater.* **2000,** *6,* 601.

32. Orimo, S.; et al. *J. Appl. Phys.* **2001**, *90*, 1545.

33. Fukunaga K.; et al. *J. Alloys Comp.* **2001**, *327*, 224.

34. Hirscher, M.; et al. *J. Alloys Comp.* **2002**, *330*, 654.

35. Atsumi, H.; Tauchi, K. *J. Alloys Comp.* **2003**, *356*, 705.

36. Imamura, H.; *J. Alloys Comp.* **2002**, *330*, 579.

37. Gregg, S.G.; Sing, K.S.W. *Adsorption, Surface Area and Porosity*, Academic Press: New York, 1982.

38. Uberuaga, B.P., et al. *Phys. Rev. Lett.* **2003**, *91*, 105901.

39. Bhatia, S. K. *Langmuir* **2002**, *18*, 6845.

40. Nguyen, T.X.; Bhatia, S.K.; Nicholson, D., *J. Chem. Phys.* **2002**, *117*, 10827.

41. Bhatia, S.K.; Tran, K.; Nguyen, T. X.; Nicholson, D. *Langmuir* **2004**, *20*, 9612.

42. Buch, V.J. *J. Chem. Phys.* **1994**, *100*, 7610.

43. Steele, W.A. *The Interaction of Gases with Solid Surfaces*, Pergamon Press, New York, 1974.

44. Honig, J.M.; Reyerson, L.H. *J. Phys. Chem.* **1952**, *56*, 140.

45. Metropolis, N.; Rosenbluth, A.W.; Rosenbluth, M.N.; Teller, A.N.; Teller, E., *J. Chem. Phys.* **1953**, *21*, 1087.

46. Adams, D.J. *Mol. Phys.* **1974**, *28*, 5.

47. Nicholson, D; Parsonage, N.G. *Computer Simulation and the Statistical Mechanics of Adsorption*, Academic Press, London, 1982.

48. Bhatia, S.K.; Nicholson, D. *J. Chem. Phys.* **2003**, *119*, 1719.

49. Avgul, N.N.; et al. *J. Coll. Int. Sci.* **1973**, *42*, 486.

50. Thanh, T.X.; Bhatia, S.K. *J. Phys. Chem. B.* **2004**, *108*, 14032.

51. Tanaka, H.; et al. *J. Phys. Chem. B.* **2004**, *108*, 17457.

52. Feynman, R.P.; Hibbs, A.R. *Quantum Mechanics and Path Integrals*, McGraw-Hill, New York, 1965.

53. Atkins, P.W. *Physical Chemistry*, Oxford University Pres, Oxford, 1994.

54. Myers, A.L.; Siperstein, F. *Coll. Surf.* **2001**, *187*, 73.

55. Sellers, H.; Gislason, J. *Surf. Sci.* **1999**, *426*, 147.

Table 1. Lennard-Jones interaction parameters employed in the simulations

Parameter	CH_4- CH_4	H_2- H_2	Silica, O-O	C-C
σ_{ii} (nm)	0.381	0.296	0.29	0.34
$\in_{ii}/k_B$ (K)	148.1	34.2	290	290

Table 2. Open pore volumes at different pore sizes in AX-21 carbon, based on fit of hydrogen adsorption data

Pore width, H_i (nm)	Center-to-center volume, v_i (cm^3/g)	Open pore volume, V_p (cm^3/g)
0.755	0.509	0.284
1.08	0.296	0.204
1.44	0	0.0
1.76	0.646	0.523

Table 3. Entropy change on adsorption of hydrogen

System	Pore width or diameter (nm)	K (bar^{-1})	$-\Delta H^o$ (kJ/mole)	$-\Delta S^o/R$
H_2 in carbon slit pore at 100 K	0.755	0.852	6.46	7.93
	1.08	0.0690	4.38	7.94
	1.44	0.0493	3.90	7.7
	1.76	0.0456	3.71	7.55
H_2 in carbon slit pore at 298 K	0.755	5.808×10^{-3}	7.56	8.20
	1.08	2.383×10^{-3}	5.23	8.15
	1.44	1.810×10^{-3}	4.54	8.15
	1.76	1.599×10^{-3}	4.21	8.14
H_2 in cylindrical silica pore at 298 K	0.65	1.137×10^{-2}	11.17	8.95
	1.04	7.207×10^{-3}	6.67	7.61
	2.39	1.847×10^{-3}	4.13	7.95
CH_4 in carbon slit pore at 298 K	0.755	8.3247×10^{-1}	22.84	9.40
	1.08	1.735×10^{-2}	14.59	9.94
	1.44	8.304×10^{-3}	11.73	9.53
	1.76	9.451×10^{-3}	10.83	9.03

List of Figure Captions

Figure 1. Slit pore having size large enough to pack two layers of adsorptive.

Figure 2. Variation of delivery with heterogeneity parameter *s* for various values of $-\Delta\bar{H}^o / RT$, for (a) H_2 and (b) CH_4.

Figure 3. (a) (9,6) nanotube, and (b) array of nanotubes in square geometry.

Figure 4. Fit of simulation to experimental data of Bénard and Chahine [9], for adsorption of hydrogen on AX-21 activated carbon. (a) Experimental and theoretical variation of gas-solid virial coefficient with temperature and, (b) experimental and simulation isotherms at various temperatures. Open symbols represent experimental data, and filled symbols the theoretical or simulation results. In (a) dashed line represents linear regression over experimental values, and inset shows the deviation of the value of the gas-solid virial coefficient at the lowest temperature of 77 K.

Figure 5. Experimental and calculated variation of delivery with temperature for hydrogen on AX-21. Symbols joined by dotted lines represent simulation values, and solid curves the experimental result. The absolute delivery is for the micropore volume of the adsorbent and does not include the gas delivered from the bulk-gas dead space inside the container.

Figure 6. Langmuir plots for adsorption of (a), (b) hydrogen adsorption in carbon slit pores of various width at 100 K and 298 K respectively, (c) hydrogen adsorption in cylindrical pores of various diameters in silica at 298 K, and (d) methane adsorption in carbon slit pores of various width at 298 K. In (d) alternate coordinates are used due to the larger value of the equilibrium constant..

(b)

Figure 7. Temperature variation of (a) specific absolute delivery, (b) isosteric heat of adsorption, (c) specific excess delivery and (d) enhancement factor, for hydrogen on activated carbons of various pore sizes.

Figure 8. Temperature dependence of (a) hydrogen delivery, and (b) isosteric heat of adsorption, for endohedral adsorption in nanotubes of various diameters.

Figure 9. (a) Absolute delivery, and (b) enhancement factor, for hydrogen from carbon nanotubes spaced 0.9 nm apart in square array.

Figure 10. Temperature variation of (a) specific absolute delivery, (b) isosteric heat of adsorption, (c) specific excess delivery and (d) enhancement factor, for methane on activated carbons of various pore sizes.

Figure 11. (a) Absolute delivery, and (b) enhancement factor, for methane from carbon nanotubes spaced 0.9 nm apart in square array.

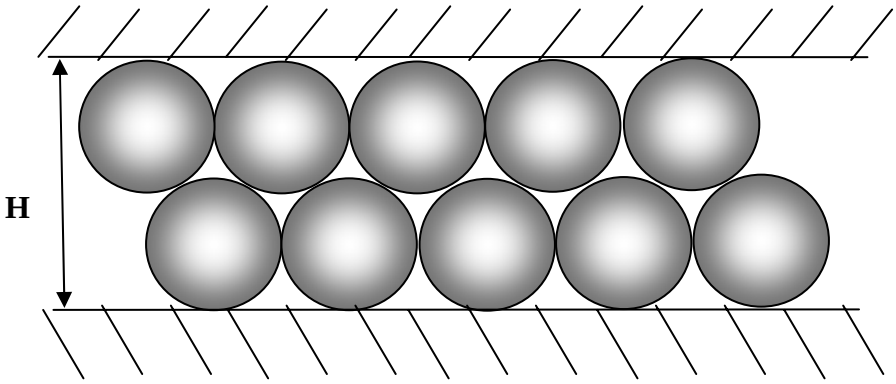

Figure 1. Slit pore having size large enough to pack two layers of adsorptive.

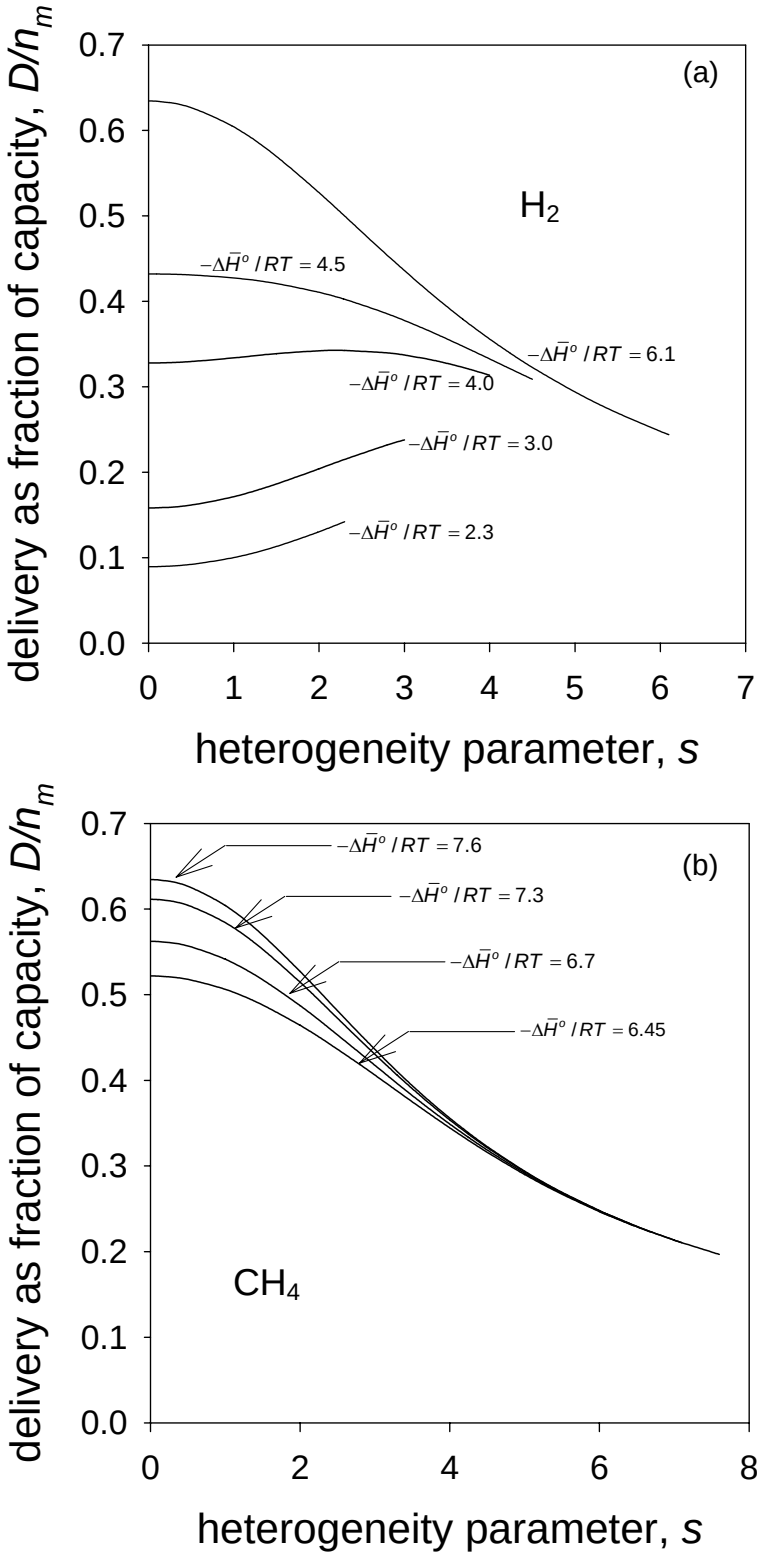

Figure 2. Variation of delivery with heterogeneity parameter *s* for various values of $-\Delta\bar{H}^o / RT$, for (a) H_2 and (b) CH_4.

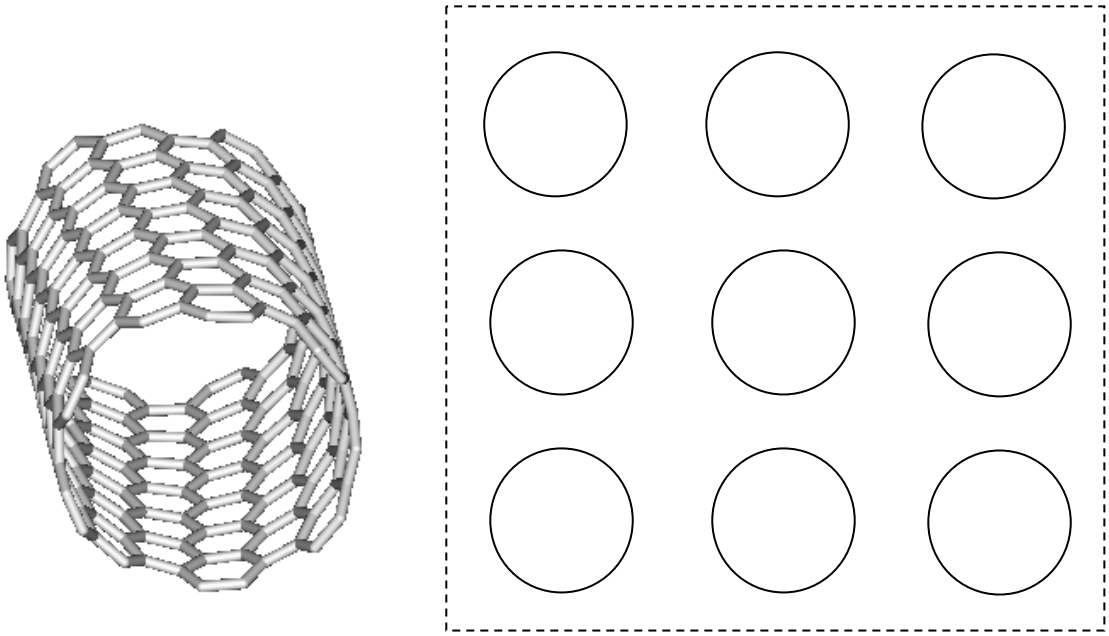

(a) (b)

Figure 3. (a) (9,6) nanotube, and (b) array of nanotubes in square geometry.

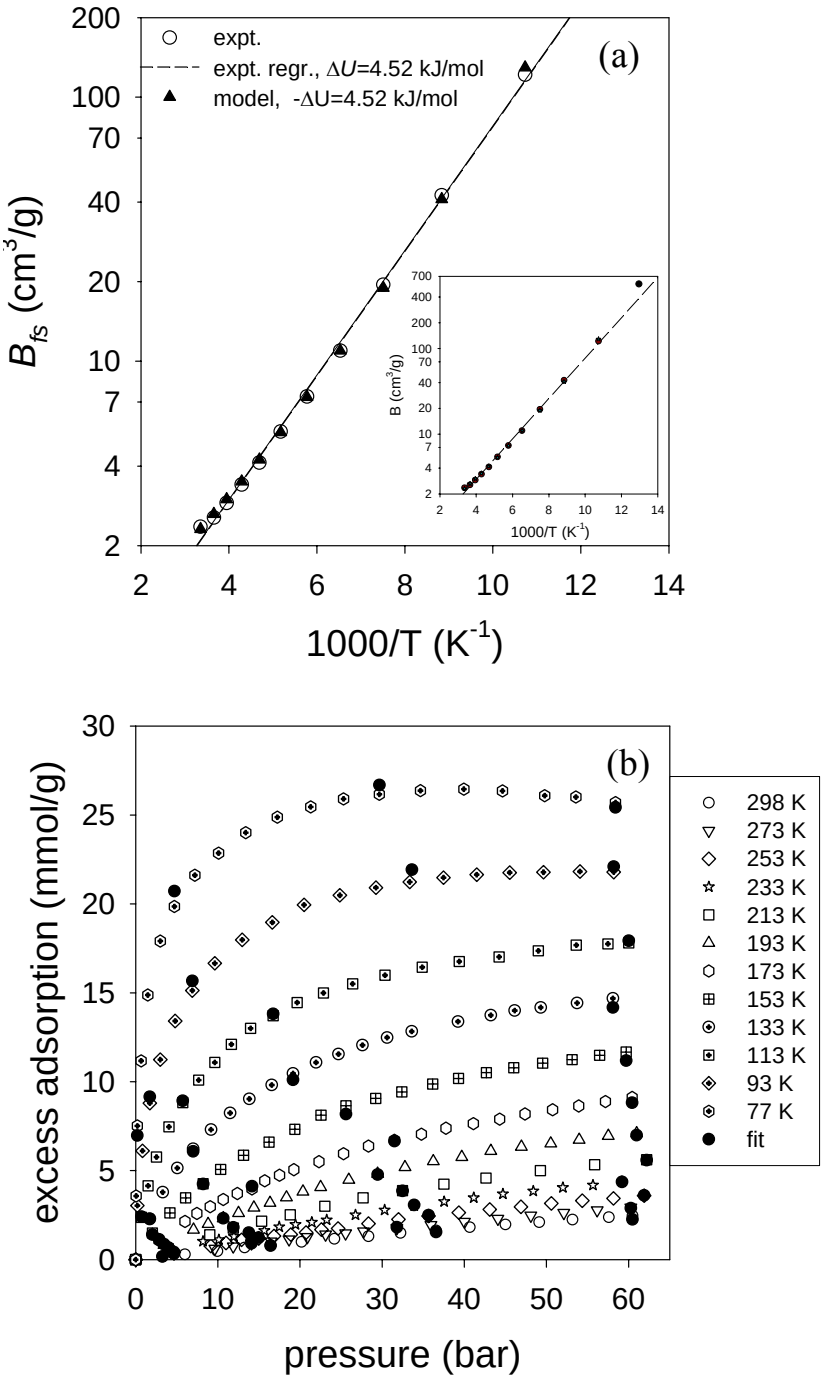

Figure 4. Fit of simulation to experimental data of Bénard and Chahine [9], for adsorption of hydrogen on AX-21 activated carbon. (a) Experimental and theoretical variation of gas-solid virial coefficient with temperature and, (b) experimental and simulation isotherms at various temperatures. Open symbols represent experimental data, and filled symbols the theoretical or simulation results. In (a) dashed line represents linear regression over experimental values, and inset shows the deviation of the value of the gas-solid virial coefficient at the lowest temperature of 77 K.

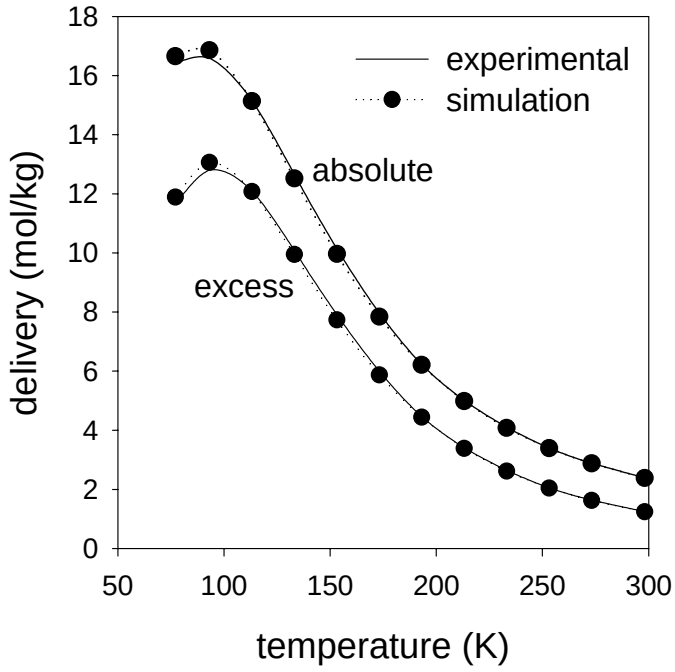

Figure 5. Experimental and calculated variation of delivery with temperature for hydrogen on AX-21. Symbols joined by dotted lines represent simulation values, and solid curves the experimental result. The absolute delivery is for the micropore volume of the adsorbent and does not include the gas delivered from the bulk-gas dead space inside the container.

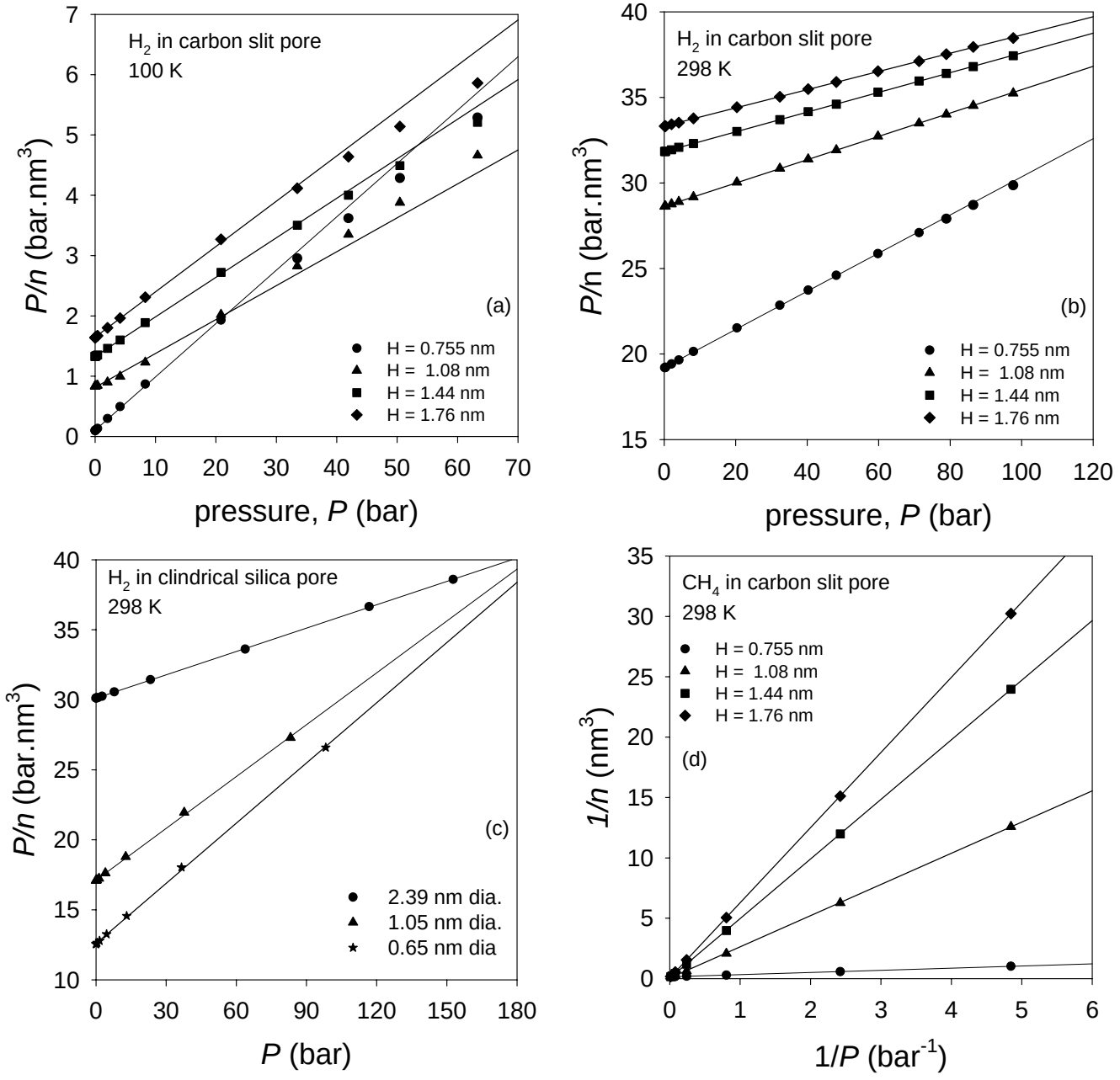

Figure 6. Langmuir plots for adsorption of (a), (b) hydrogen adsorption in carbon slit pores of various width at 100 K and 298 K respectively, (c) hydrogen adsorption in cylindrical pores of various diameters in silica at 298 K, and (d) methane adsorption in carbon slit pores of various width at 298 K. In (d) alternate coordinates are used due to the larger value of the equilibrium constant..

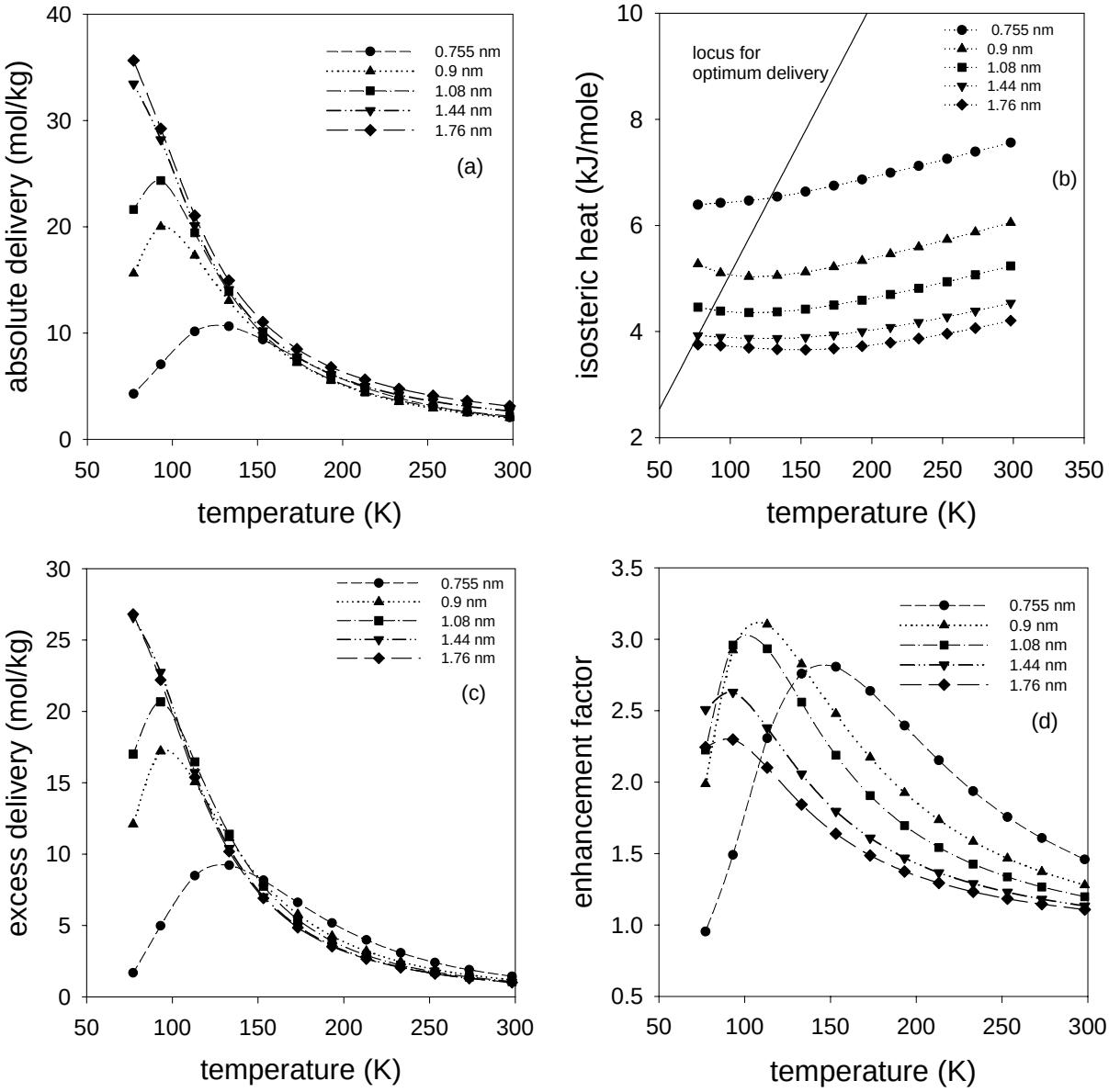

Figure 7. Temperature variation of (a) specific absolute delivery, (b) isosteric heat of adsorption, (c) specific excess delivery and (d) enhancement factor, for hydrogen on activated carbons of various pore sizes.

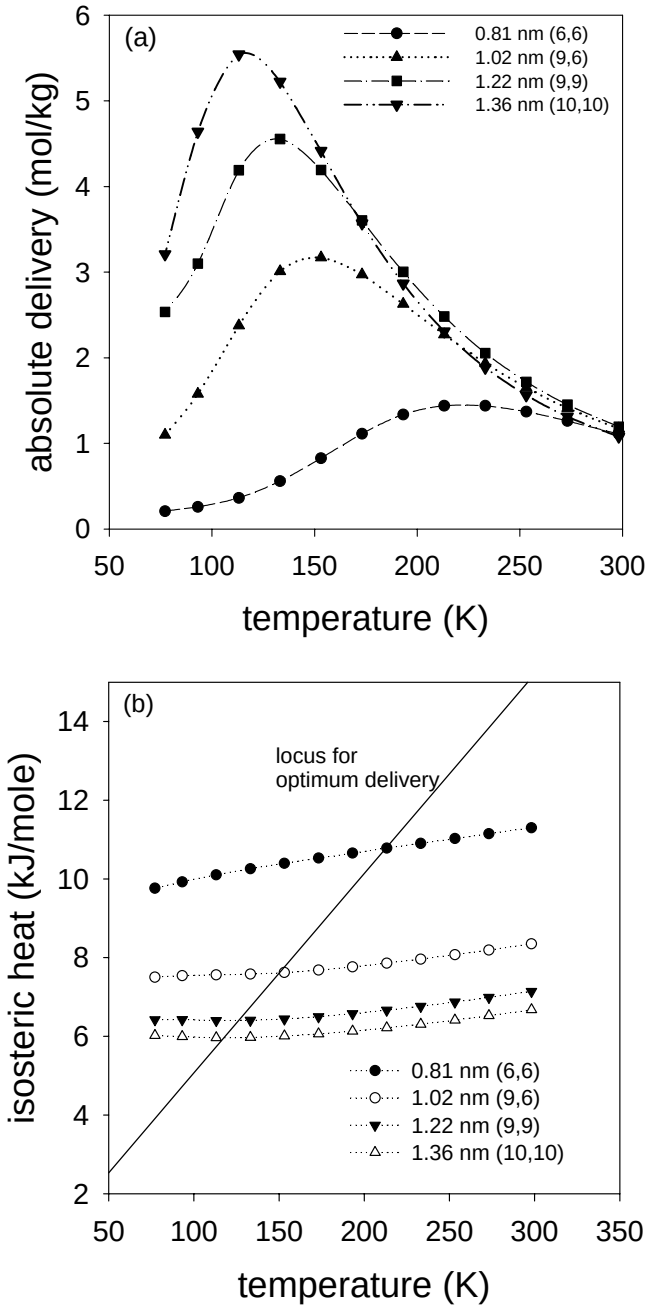

Figure 8. Temperature dependence of (a) hydrogen delivery, and (b) isosteric heat of adsorption, for endohedral adsorption in nanotubes of various diameters.

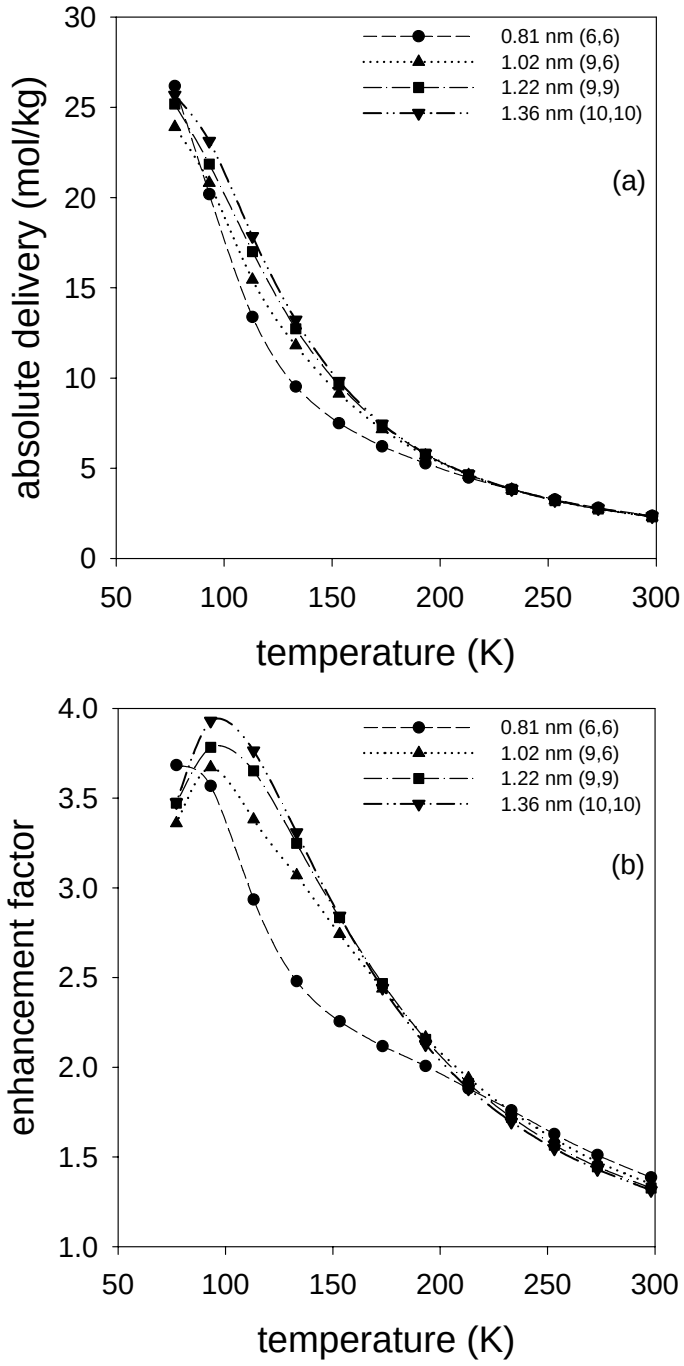

Figure 9. (a) Absolute delivery, and (b) enhancement factor, for hydrogen from carbon nanotubes spaced 0.9 nm apart in square array.

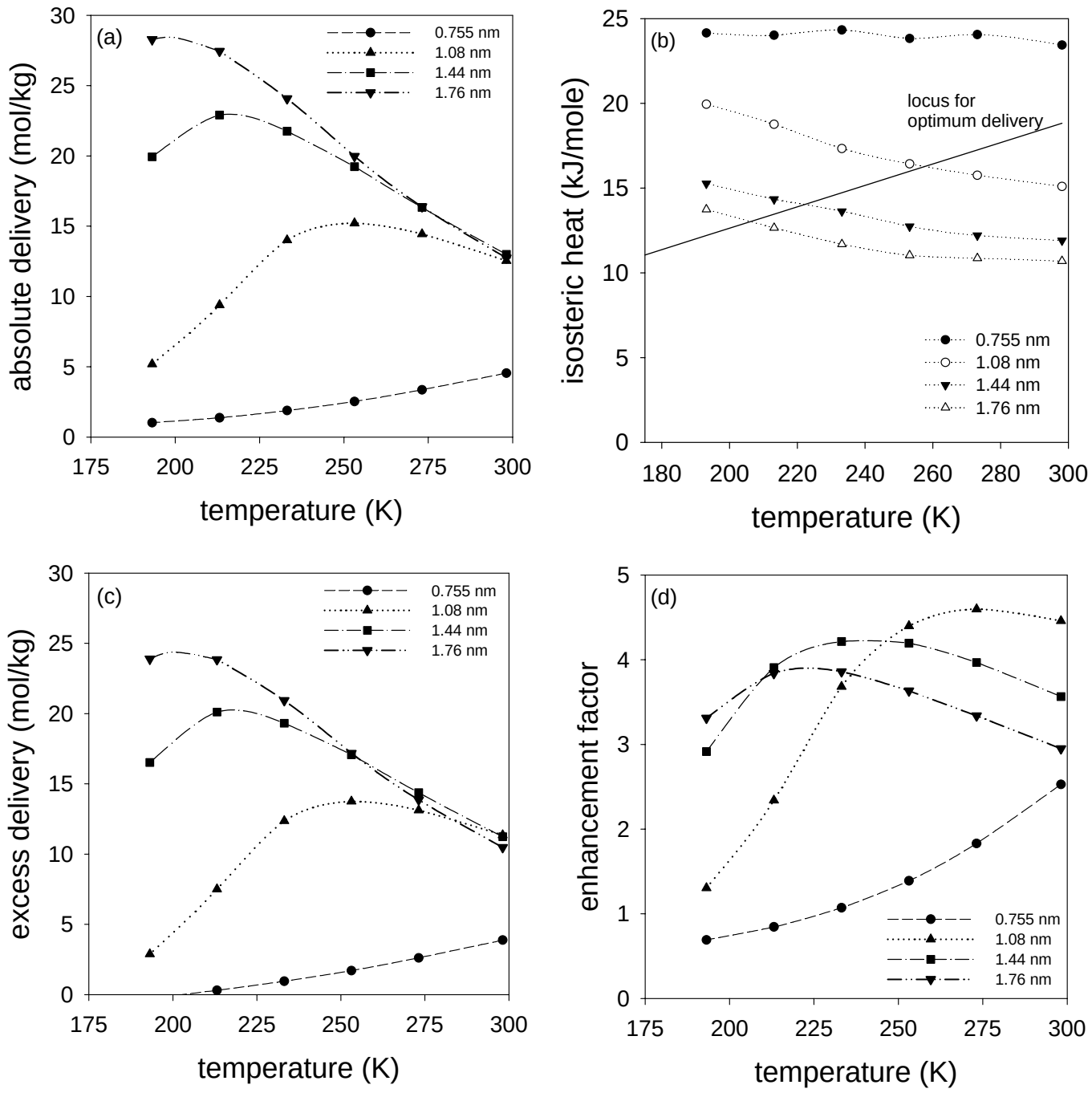

Figure 10. Temperature variation of (a) specific absolute delivery, (b) isosteric heat of adsorption, (c) specific excess delivery and (d) enhancement factor, for methane on activated carbons of various pore sizes.

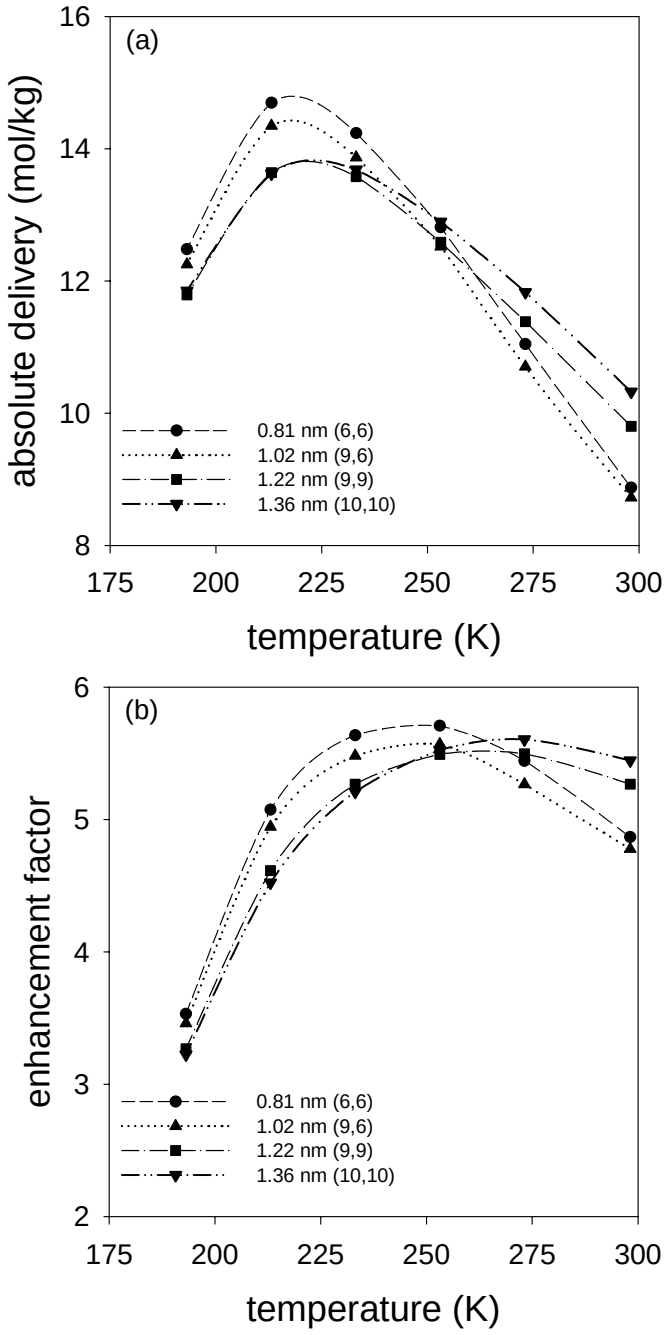

Figure 11. (a) Absolute delivery, and (b) enhancement factor, for methane from carbon nanotubes spaced 0.9 nm apart in square array.